ASM Sc. J., 21(1), 2026

https://doi.org/10.32802/asmscj.2026.0015

The Biocompatibility of Synthesised Hydroxyapatite (HAp) Originating from The *Meretrix lyrata* Shell Investigated as A Functional Component in UV Filters Formulations

M.S. Azhar[1], M.Z.H. Rozaini[1], M.H. Razali[2], M.U. Osman[2] and M.S. Zulhadi[1]

[1]*Faculty of Fisheries and Aquaculture Sciences, University Malaysia Terengganu, Terengganu, Malaysia*

[2]*Faculty of Science and Marine Environment, University Malaysia Terengganu, Terengganu, Malaysia*

The escalating necessity for safer and ecologically benign sunscreen formulations has prompted the exploration of alternative UV-filtering agents to supplant traditional titanium dioxide (TiO_2) and zinc oxide (ZnO), which bring forth concerns regarding cytotoxicity, environmental durability, and potential harm to coral reefs. In the present investigation, hydroxyapatite (HAp) was synthesised from the shells of *Meretrix lyrata* clams and examined as a functional constituent in UV filter formulations. For the intention of enhancing UV absorption attributes, HAp experienced doping with iron (Fe) and manganese (Mn). The formed materials were evaluated through techniques like Nuclear Magnetic Resonance (NMR), Fourier Transform Infrared Spectroscopy (FTIR), X-Ray Diffraction (XRD), and Scanning Electron Microscopy (SEM), thereby substantiating their crystalline layout and nanostructured characteristics. UV-Vis spectrometry methods were utilised to measure UV light absorption, showing that emulsions with HAp doping displayed a broader absorbance range in contrast to standard HAp. There was a noticeable connection between UV absorbance and SPF values, with HAp-Mn securing a distinguished SPF of 35. These results underscore the viability of Fe- and Mn-doped biogenic HAp as a sustainable and reef-safe alternative for the development of next-generation sunscreen formulations.

Keywords: Ultraviolet (UV) filters; hydroxyapatite (HAp); *Meretrix lyrata*

I. INTRODUCTION

The climbing statistics of skin problems connected with ultraviolet (UV) radiation have greatly escalated the requirement for effective and secure sunscreen formulations. In traditional formulations, sunscreen relies on active components that either absorb or reflect harmful ultraviolet radiation. These active components are generally categorised into three distinct classifications: (1) physical (inorganic) filters, such as titanium dioxide (TiO_2) and zinc oxide (ZnO), which serve to reflect and scatter UV rays and are often noticeable as a white layer upon the skin; (2) chemical (organic) filters, which mitigate UV radiation via molecular excitation; and (3) nano-particulate filters, wherein inorganic materials such as TiO_2 and ZnO are manipulated at the nanoscale (Serpone, 2021; Kera *et al.*, 2024). Significantly, upon reduction to nanoparticle dimensions, these substances cease to function predominantly through reflection and scattering; rather, they primarily absorb UV radiation owing to their semiconductor bandgap characteristics (Banerjee, 2011; Reinosa *et al.*, 2016). Recent investigations have indicated that nano-sized TiO_2 and ZnO reflect less than 5% of UV radiation, thereby operating similar to chemical filters as opposed to authentic physical barriers (Cole *et al.*, 2016). Despite their extensive utilisation, both TiO_2 and ZnO, especially in their nano-form, have evoked alarms regarding their environmental persistence, photocatalytic behavior, as well as potential cytotoxic effects (Gackowski *et al.*, 2023;

*Corresponding author's e-mail: mohamad.safuan@umt.edu.my

Bhardwaj *et al.*, 2023). Additionally, various chemical UV filters have shown associations with endocrine disruption and harmful consequences on coral reef ecosystems (Watkins & Sallach, 2021; Moeller *et al.*, 2021). This condition has led to a global exploration for alternative, nature-friendly, and biocompatible UV-filter solutions. Hydroxyapatite (HAp), a naturally occurring bioceramic characterised by the chemical formula $Ca_{10}(PO_4)_6(OH)_2$, has emerged as a compelling candidate for both cosmetic and biomedical applications, attributed to its exemplary biocompatibility, non-toxicity, and adjustable surface properties (Singh *et al.*, 2020; Gul & Albayrak, 2024; Wang *et al.*, 2025). Past research has emphasised its ability for UV absorption; however, its study as a UV filter in sunscreen blends is narrow. Interestingly, embracing biogenic origins for the creation of HAp introduces an eco-conscious strategy, ensuring effective resource management and imaginative functionality.

This research presents an innovative methodology by synthesising hydroxyapatite from *Meretrix lyrata*, a marine clam species, with the objective of formulating an alternative active ingredient for sunscreen applications. The powders of biogenic hydroxyapatite, in both their raw form and those enriched with iron (Fe) and manganese (Mn) ions, were systematically investigated for their prospective use as ultraviolet (UV)-resistant materials. The method of doping is perceived to strengthen the optical absorption traits of hydroxyapatite by adjusting its electronic structure, leading to greater utility as a UV filter. To address the prevailing research deficit, this study offers an extensive assessment of the synthesised materials, encompassing their physicochemical attributes characterised through Nuclear Magnetic Resonance (NMR), Fourier Transform Infrared Spectroscopy (FTIR), X-Ray Diffraction (XRD), and Scanning Electron Microscopy (SEM). This review seeks to detail the resilience of structures, the features of crystallinity, the surface functional groups that play a role, and the particle arrangement, which are vital components that impact the performance of UV-blocking and skin compatibility.

This investigation is valuable as it can yield a biocompatible, sustainable for the environment, and robust alternative to usual inorganic sunscreen formulations. By employing waste clam shells as the calcium precursor for hydroxyapatite synthesis, this strategy not only addresses environmental sustainability concerns but also aligns with contemporary trends that favour natural and reef-safe sun protection products. Moreover, the examination of Fe and Mn doping offers an avenue to optimise the optical characteristics of hydroxyapatite, potentially equalling or surpassing the UV protective efficacy of titanium dioxide (TiO_2) and zinc oxide (ZnO) while mitigating their associated limitations. In conclusion, this inquiry broadens the developing field of knowledge regarding functional biomaterials for cosmetic functions, furnishing vital revelations about the growth of next-generation UV filters that underscore the importance of both human health and environmental care.

II. MATERIALS AND METHOD

A. Synthesis of Hydroxyapatite (HAp) from Meretrix lyrata Shells

The clam shells underwent extensive cleaning, boiling, and drying for one hour. The dried shells were then ground and sieved. Calcium carbonate was calcined at 1000 °C for four hours to yield calcium oxide. Stoichiometric hydroxyapatite was synthesised by combining 0.25 M calcium and 0.15 M phosphorus precursors, achieving a Ca/P ratio of 1:6. Distilled water was mixed with CaO to create a calcium hydroxide solution, serving as the calcium precursor. The solution's pH was maintained at 12 whiles being stirred at 400 rpm for one hour. The phosphorus precursor was diluted and mixed to maintain a pH of approximately 2.0. The prepared phosphoric acid solution was added to the calcium hydroxide solution to commence titration. The mixture was vigorously stirred at 700 rpm for thirty minutes. The pH was then adjusted to 10 by incorporating ammonium hydroxide. The mixture was aged for 21 hours and stirred magnetically at 500 rpm for an hour post-titration to yield a white precipitate. The precipitates underwent vacuum filtration using an aspirator pump. After 16 hours of drying at 100 °C, the precipitate was sieved, rinsed with deionised water, and drying at 100 °C before it was calcined at 700 °C.

B. Doping with Fe and Mn

In the context of doping with iron (Fe) and manganese (Mn), an analogous procedure was employed, incorporating of $Fe(NO_3)_3 \cdot 9H_2O$ for the synthesis of iron-doped hydroxyapatite (HAp) and of $Mn(NO_3)_2$ for the production of manganese-doped HAp during the reaction phase. The modified samples experienced a comparable aging process, which was succeeded by filtration, drying, and calcination.

C. Emulsification of samples

The formulation is delineated into the oil phase and the aqueous phase throughout the emulsification procedure. The petroleum jelly, serving as a thickening agent, along with the surfactants, was integrated within the oil phase following a heating process to 70 °C. Concurrently, distilled water was subjected to a similar heating process, also reaching 70 °C. Upon achieving the requisite temperature in both components, the oil phase is introduced into the aqueous phase solution while being subjected to vigorous agitation. Once the amalgamation attains a state of homogeneity, it is systematically stirred using a mechanical stirrer until the temperature diminishes to 35 °C. The samples were subsequently preserved in a cool and dark environment. The samples were evaluated daily to detect any potential modifications. The most stable emulsions were infused with undoped HAp, doped HAp-Fe, and HAp-Mn for subsequent analysis. The samples were evaluated daily to detect any potential modifications.

D. Characterisations

The synthesised powders underwent an extensive evaluation through the application of these methodologies: the stability of the phosphate groups was substantiated via NMR spectroscopy, spectral data were obtained through the application of FTIR spectroscopy, encompassing the range from 3700 to 400 cm^{-1} to identify functional groups. XRD spectroscopy utilised Cu-Kα radiation to elucidate the crystallinity and phase purity of the materials. SEM microscopies investigate the particle morphology with 1,000x and 5,000x magnification. Three replicates were performed for each sample.

D. UV-Spectrometry Testing and Sun Protection Factor (SPF) calculation

The efficacy of the UV filter was assessed using an in vitro UV-visible spectrophotometric technique. Each microemulsion sample was accurately weighed, placed in a volumetric flask, and diluted with ethanol. The solution underwent homogenisation with an ultrasonicator for five minutes. The homogenised samples were filtered, discarding the initial 10 mL. A 5.0 mL aliquot was transferred to a 50 mL volumetric flask and diluted with ethanol. Each aliquot was sealed in vials and stored at 25 °C in darkness. The formulations were scanned at intervals with ethanol as a blank. Three replicates were performed for each sample. Absorbance values were recorded weekly over 28 days to evaluate UV effects. The SPF was calculated using the Mansur equation after the measurements were completed (Hermund *et al.*, 2022):

$$SPF = CF \, x \sum_{290}^{320} EE(\lambda) \, x \, I(\lambda) \, x \, A(\lambda) \quad (1)$$

where CF: Correction factor, a constant value used in the calculation; EE(λ): Erythemal effect of radiation at a specific wavelength (λ), which is the ability of UV radiation to cause sunburn; I(λ): Intensity of the solar spectrum at a specific wavelength (λ); A(λ): Absorbance of the sunscreen at a specific wavelength (λ).

III. RESULTS AND DISCUSSIONS

A. Percentage yield

The yield of undoped hydroxyapatite (undoped HAp) was 76.8 ± 0.3, while doped hydroxyapatite with manganese (doped HAp-Mn) and doped hydroxyapatite with iron (doped HAp-Fe) yields were 85.06 ± 0.25 and 80.03 ± 0.49, respectively as shown in Table 1. Various factors, including processing phases, container types, and storage conditions, may affect the yield differences of each shell. The doped HAp-Fe sample exhibited the highest moisture content (11.99 ± 0.08), whereas undoped HAp and doped HAp-Mn showed lower levels (10.18 ± 0.06 and 8.32 ± 0.03, respectively). This phenomenon may be attributed to the hydroxyapatite yield initiated during extraction which involved the mild conditions employed during undoped HAp extraction. Such conditions entailed low-temperature hot water extraction and a moderate NaCl concentration for pre-treatment.

Furthermore, all samples-maintained pH values around 7.1, indicating neutrality.

Table 1. Percentage yield of extracted, moisture and pH readings *Meretrix lyata* shell

Sample	Percentage yield (%)	Moisture (%)	pH (%)	Sample
Undoped HAp	76.8 ± 0.3	8.32 ± 0.03	7.13 ± 0.12	76.8 ± 0.3
Doped HAp-Fe	85.06 ± 0.25	11.99 ± 0.08	7.13 ± 0.15	85.06 ± 0.25
Doped HAp-Mn	80.03 ± 0.49	10.18 ± 0.06	7.16 ± 0.15	80.03 ± 0.49

Values are the mean ± standard deviation of n=3 with P<0.05

B. Structural Characterisations

NMR analysis detected of a singular proton in HAp (δH = 1.537 ppm), derived from unmodified HAp sourced from *Meretrix lyata* clam shell, was confirmed via 1H NMR spectroscopy as in Figure 1. This proton aligns with the chemical composition of Calcium Carbonate. Furthermore, an additional singlet resonance was noted on the left of the proton spectra exhibited a chemical shift of δH 7.261 ppm, attributed to the solvent utilised in the spectroscopy.

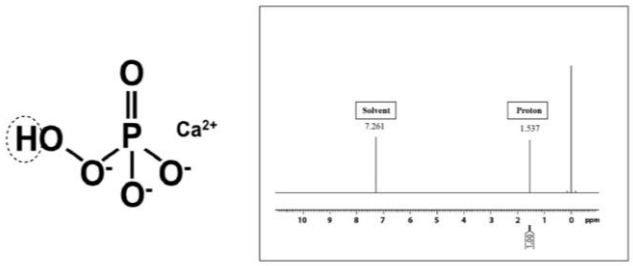

Figure 1. Single Proton (1H NMR) in Calcium Carbonate (Hydroxyapatite) marked in dotted circle.

The FTIR spectra of undoped HAp, doped HAp-Fe, and doped HAp-Mn were presented in Figures 2. Generally, the spectra exhibit a pronounced decline peak between 1400 and 4100 cm^{-1}, along with broad waves up to 3600 cm^{-1}. It can be concluded that the phosphonate (PO) group was identified within the spectral range of 400 – 900 cm^{-1}, exhibiting various modes, specifically, the bending modes of the PO group. The bending mode associated with the hydroxyl (O-H) group was observed within the range of 1600 – 1700 cm^{-1}, attributed to the presence of moisture retained in the calcined clam shell. It can also be inferred that there was no alkyl groups present in the spectrum, thereby suggesting the absence of residual organic materials. The residual-free O-H stretching was observed between 3600 – 3700 cm^{-1} across all spectra analysed.

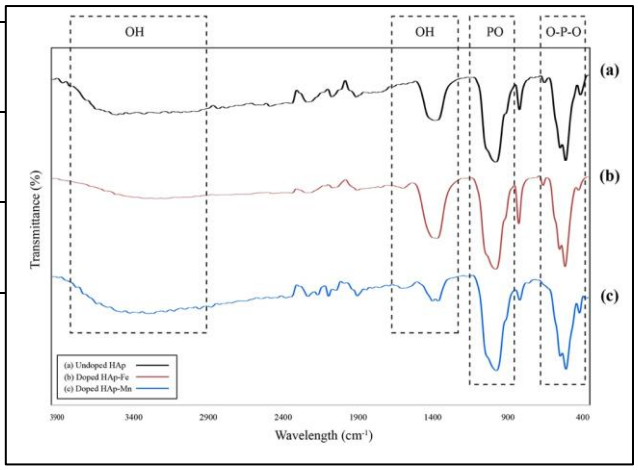

Figure 2. The FTIR spectra of (a) undoped HAp, (b) doped HAp-Fe, and (c) doped HAp-Mn

Figure 3 represent the XRD patterns of the undoped HAp, doped HAp-Fe and doped HAp-Mn samples, exhibit a remarkable correspondence with the Joint Committee on Powder Diffraction Standards (JCPDS) pattern #74-566 for hydroxyapatite (Rasterelli *et al.*, 2012; de Araujo *et al.*, 2007).

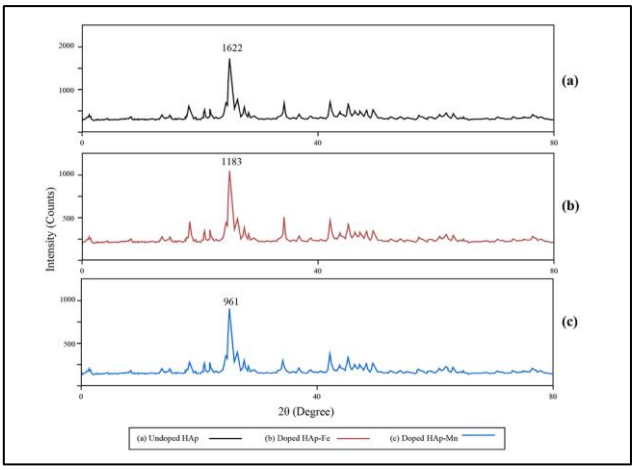

Figure 3. X-ray diffraction pattern of (a) undoped HAp, (b) doped HAp-Fe and (c) doped HAp-Mn

As presented in Table 2, all samples exhibited similar crystalline peak at about 29.29° but different in intensity counts. All analysed samples exhibit similar crystalline peak values ranging from approximately 3.046 Å to 3.047 Å at an

angle of 29.29°, yet they show significant variations in intensity counts. The undoped HAp recorded an intensity count of 1622°, followed by the doped HAp-Fe at 1183° and the doped HAp-Mn at a lower count of 961°. An elevated peak intensity suggests a higher atomic presence in the crystalline structure, potentially indicating improved crystallinity or larger crystal dimensions. The incorporation of Fe^{3+} and Mn^{2+} ions into hydroxyapatite leads to decreased crystallinity, as extensively documented (Lala *et al.,* 2015; Liu *et al.,* 2021).

The median crystallite dimensions for undoped hydroxyapatite (HAp) alongside its doped variants, HAp-Fe and HAp-Mn. A comparative analysis reveals that the undoped variant has the largest crystallite size at 103.39 nm, whereas the doped HAp-Fe variant measures 97.94 nm, and doped HAp-Mn has the smallest at 84.69 nm. This observation suggests that dopants likely substitute for calcium ions at sites with a radius of approximately 0.99 Å, given the larger charges and smaller ionic radii of Mn^{2+} (0.63 Å) and Fe^{3+} (0.64 Å). Additionally, it is important to note that other ions with smaller ionic radii than Ca^{2+} have been shown to inhibit hydroxyapatite formation (Herzog *et al*., 2024).

Table 2. The XRD data of undoped HAp, doped HAp-Fe and doped HAp-Mn powder

Sample	2θ	Highest Crystalline Peak (d, Å)	Intensity Counts°	Crystallite size (nm)
Undoped HAp	29.29	3.047	1622	103.39
Doped HAp-Fe	29.29	3.047	1183	97.94
Doped HAp-Mn	29.29	3.046	961	84.69

Figure 4 illustrates the microstructural SEM images of undoped HAp, doped HAp-Fe, and doped HAp-Mn at magnifications of 1,000x and 5,000x. At magnification of 5,000x, Figure 4(d) shows that the undoped HAp displayed weaker structural integrity relative to the other samples in Figures 4(e) and 4(f). This observation suggests a reduced number of linkages and an increase in pore size, potentially arising from a compromised intercalating framework. Intercalation refers to the insertion of molecules or ions between the layers of a material. Under certain conditions, intercalation may lead to structural expansion, resulting in increased voids or pores between layers (Roth *et al*., 2016). The presence of larger pores could enhance permeability or surface area, thereby affecting the material's properties and potential applications.

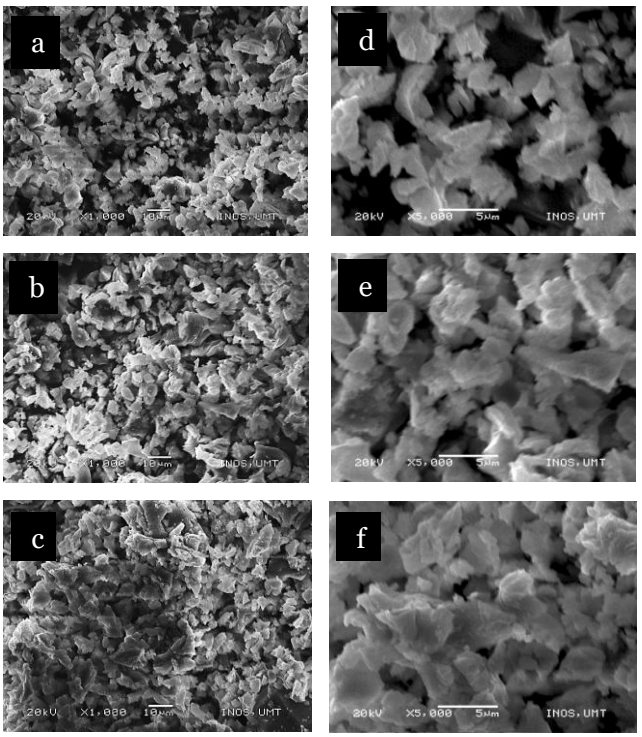

Figure 4. SEM imaging of (a) undoped HAp, (b) doped HAp-Mn and (c) doped HAp-Fe powder using SEM with 1,000x magnification. SEM imaging of (d) undoped HAp, (e) doped HAp-Mn, and (f) doped HAp-Fe powder using SEM with 5,000x magnification.

A close packed calcium structure with small pores was identified in doped HAp-Fe and doped HAp-Mn samples. This observation enhances the strand value of Ferum and Manganese metal chelation structures in both instances. High strand value chelating compounds can enhance metal ion selectivity, stability, and kinetic properties, rendering them advantageous for diverse applications (Gulcin & Alwasel, 2022). High strand value metal ion chelation significantly enhances arrangement properties, with denser strands in doped HAp exhibiting superior strength compared to looser undoped strands.

C. UV Absorption Performance and SPF

The absorbance values for undoped HAp, doped HAp-Fe and doped HAp-Mn demonstrate a linear reduction from 290 nm to 320 nm wavelength, as delineated in Figure 5. The incorporation of dopants (specifically Fe and Mn) into Hydroxyapatite (HAp) has resulted in notable alterations. as seen in Figure 4. The selection of these metals is substantiated by the research conducted by de Araujo *et al.* (2010), which demonstrated that iron and manganese can enhance the ultraviolet (UV) absorption spectrum. The HAp-Mn emulsion exhibits an absorption band that spans from UV to the visible spectrum (290-320 nm), commencing at a value of 4.356. In contrast, the HAp-Fe emulsion showcases an absorption band ranging from UV to the visible spectrum (267-650 nm), beginning at a value of 3.557, which is subsequently followed by the undoped HAp and control emulsions at values of 2.813 and 2.297, respectively. This data signifies that the incorporation of HAp as an organic constituent within a sunscreen emulsion can lead to an enhanced absorption band in comparison to the emulsion alone. Furthermore, the introduction of inorganic dopants such as Fe and Mn has augmented the absorption capacity beyond that of the HAp emulsion by itself (Rozaini *et al.*, 2017). The formulation's components and their interactions likely contribute to a stable composition, resulting in an elevated calculated SPF value.

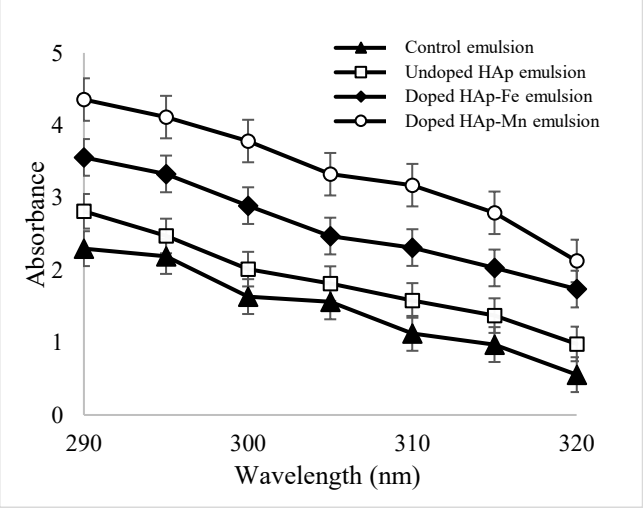

Figure 5. Absorption spectra of the photoprotective emulsion formulations

As awareness of UV radiation's harmful effects increases, this study highlights the importance of photoprotective emulsions with marine extracts for skin protection. It is essential to develop an optimal formulation of photoprotective emulsion using HAp from clam shells that is photostable, non-irritating, and non-toxic to reduce UV-induced skin damage. The efficacy of photoprotective emulsions is significantly determined by their SPF value. The UV spectrophotometric technique is the preferred in vitro method for SPF evaluation due to its efficiency, simplicity, and cost-effectiveness (Dutra *et al.*, 2004). Additionally, the application of the Mansur equation is deemed pragmatic for SPF determination in photoprotective emulsions. Moreover, this recommended methodology serves as a straightforward quality control measure in the production of photoprotective emulsions, thus being relevant for assessing both organic and inorganic formulations. All the calculated SPF values of control, undoped HAp, doped HAp-Fe and doped HAp-Mn emulsions are shown in Table 3.

Table 3. Calculated SPF values of the formulation of the photoprotective emulsion

Samples	Active Ingredients (AI)	Amount (%)	SPF
Undoped HAp	HAp	0	14.969 ± 2.03
Doped HAp-Fe	HAp-Fe	10.0	18.453 ± 2.40
Doped HAp-Mn	HAp-Mn	10.0	25.989 ± 3.35

Based on Table 3, Sample doped HAp-Mn exhibited a calculated SPF values of 34.427, corresponding to SPF 35. This trend was reflected in the lower SPF values of doped HAp-Fe (SPF 25) at 25.989 SPF and undoped HAp at 18.453 SPF (SPF 20). The control sample, lacking active photoprotective agents, showed the lowest SPF value of 14.969, thus classified as SPF 15. Each sample formulation evaluated in this study exhibited distinct SPF values exceeding 20, except for control emulsion. The observed variations in formulation data may be linked to the microemulsified system and the specific active ingredients employed, which possess photoprotective properties.

The UV absorption results are linked to SPF values. HAp enhances UV light absorption in protective emulsions. Inorganic dopants like Fe and Mn impede UV light penetration. The hybrid formulation markedly improves UV absorption and SPF values (Rozaini *et al.*, 2017). The HAp-emulsion demonstrates superior UV absorption relative to the blank emulsion. Undoped HAp shows diminished UV absorption compared to doped variants, HAp-Fe and HAp-Mn. Furthermore, interactions among components and formulation concentrations may elucidate variations in SPF values (Villalobos-Hernandez & Müller-Goymann, 2006). Doped HAp-Mn exhibits increased UV transmission, and a higher SPF compared to both doped HAp-Fe and undoped HAp. Discrepancies in SPF calculations may stem from the metal-to-vehicle interface and the concentration of the emulsion formulation (Rozaini *et al.*, 2017). SPF values in protective emulsions are influenced by compound concentration, solvent types, emulsion types, and component interactions (Caswell, 2001; Barnes *et al.*, 2021). Additional factors include emulsion characteristics, effects of vehicle components, inclusion of active ingredients, pH levels, and rheological properties affecting UV absorption in protective formulations (Dutra *et al.*, 2004; Kaur & Saraf, 2010; Bikiaris *et al.*, 2023).

IV. CONCLUSION

In conclusion, the undoped HAp as well as the doped formulations of doped HAp-Fe and doped HAp-Mn emulsions, were successfully synthesised utilising the clamshell species known as *Meretrix lyrata*. XRD patterns confirmed that all samples exhibit a relatively high degree of crystalline intensity, nevertheless, the intensity counts corresponding to doped HAp-Fe and doped HAp-Mn were observed to be reduced in comparison to those of the undoped HAp, attributable to the incorporation of reduced quantities of Mn into the HAp lattice. FTIR spectra revealed the presence of phosphate groups (PO_4^{3-} stretching and PO_4^{3-} bending), which correspond to the characteristics of hydroxyapatite. The incorporation of iron and manganese did not alter the fundamental functional groups present.

The doped HAp-Mn demonstrated the most significant ultraviolet (UV) absorption, followed by the doped Hap-Fe, and subsequently the undoped HAp. These UV absorbance bands are directly correlated with the SPF values, where the doped HAp-Mn formulation demonstrates an elevated SPF value of 34.427.

This investigation proficiently synthesised biogenic hydroxyapatite derived from *Meretrix lyrata* shells and elucidated its potential as an environmentally sustainable, biocompatible ultraviolet filter suitable for sunscreen applications. The incorporation of iron and manganese ions considerably enhanced the ultraviolet absorption properties while preserving biocompatibility. The manganese-doped hydroxyapatite, specifically, demonstrated promising ultraviolet-blocking efficacy comparable to conventional titanium dioxide and zinc oxide-based filters, with the additional benefits of diminished particle size and natural provenance. These findings provide a fundamental basis for the progression of sustainable, reef-safe, and effective sun-protective formulations utilising marine-derived bioceramics.

V. ACKNOWLEDGEMENT

The authors would like to express their gratitude to the Ministry of Higher Education Malaysia for funding this research via Fundamental Research Grant Scheme (FRGS), grant number FRGS/1/2024/STG05/UMT/02/4 (VOT59780). The authors also thank Universiti Malaysia Terengganu for the provision of facilities and instrumentation that render this significant research feasible and efficacious.

I. REFERENCES

Banerjee, AN 2011, 'The design, fabrication, and photocatalytic utility of nanostructured semiconductors: focus on TiO2-based nanostructures', Nanotechnology, science and applications, pp. 35–65.

Barnes, TM, Mijaljica, D, Townley, JP, Spada, F & Harrison, IP 2021, 'Vehicles for drug delivery and cosmetic moisturizers: review and comparison', Pharmaceutics, vol. 13, no. 12, p. 2012.

Bhardwaj, LK, Rath, P & Choudhury, M 2023, 'A comprehensive review on the classification, uses, sources of nanoparticles (NPs) and their toxicity on health', Aerosol Science and Engineering, vol. 7, no. 1, pp. 69–86.

Bikiaris, ND, Koumentakou, I, Hatzistamatiou, K, Lykidou, S, Barmpalexis, P & Nikolaidis, N 2023, 'Preparation and investigation of the SPF and antioxidant properties of O/W and W/O emulsions containing vitamins A, C and E for cosmetic applications', Cosmetics, vol. 10, no. 3, p. 76.

Caswell, M 2001, 'Sunscreen formulation and testing', Cosmetics and Toiletries, vol. 116, no. 9, pp. 49–60.

Cole, C, Shyr, T & Ou-Yang, H 2016, 'Metal oxide sunscreens protect skin by absorption, not by reflection or scattering', Photodermatology, photoimmunology & photomedicine, vol. 32, no. 1, pp. 5–10.

Dutra, EA, Oliveira, DAGDC, Kedor-Hackmann, ERM & Santoro, MIRM 2004, 'Determination of sun protection factor (SPF) of sunscreens by ultraviolet spectrophotometry', Revista Brasileira de Ciências Farmacêuticas, vol. 40, pp. 381–385.

Gackowski, M, Osmałek, T, Froelich, A, Otto, F, Schneider, R & Lulek, J 2023, 'Phototoxic or photoprotective? — advances and limitations of titanium (IV) oxide in dermal formulations—a review', International Journal of Molecular Sciences, vol. 24, no. 9, p. 8159.

Gul, C & Albayrak, S 2024, 'Hydroxyapatite ceramic-polymer composites for biomedical applications', in Fiber and Ceramic Filler-Based Polymer Composites for Biomedical Engineering, Springer Nature Singapore, Singapore, pp. 175–192.

Gulcin, İ & Alwasel, SH 2022, 'Metal ions, metal chelators and metal chelating assay as antioxidant method', Processes, vol. 10, no. 1, p. 132.

Hermund, DB, Torsteinsen, H, Vega, J, Figueroa, FL & Jacobsen, C 2022, 'Screening for new cosmeceuticals from brown algae Fucus vesiculosus with antioxidant and photo-protecting properties', Marine Drugs, vol. 20, no. 11, p. 687.

Herzog, BM 2024, Surfactant-enhanced in-situ chemical oxidation: developing a remediation design with experimental upscaling, Eigenverlag des Instituts für Wasser-und Umweltsystemmodellierung der Universität Stuttgart, Stuttgart.

Kera, NH, Pillai, SK & Ray, SS 2024, Inorganic ultraviolet filters in sunscreen products, Springer Nature Switzerland, viewed <https://doi.org/10.1007/978-3-031-64114-5>.

Lala, S, Ghosh, M, Das, PK, Kar, T & Pradhan, SK 2015, 'Mechanical preparation of nanocrystalline biocompatible single-phase Mn-doped A-type carbonated hydroxyapatite (A-cHAp): effect of Mn doping on microstructure', Dalton Transactions, vol. 44, no. 46, pp. 20087–20097.

Liu, FC, Grimsrud, TK, Veierød, MB, Robsahm, TE, Ghiasvand, R, Babigumira, R & Stenehjem, JS 2021, 'Ultraviolet radiation and risk of cutaneous melanoma and squamous cell carcinoma in males and females in the Norwegian Offshore Petroleum Workers cohort', American Journal of Industrial Medicine, vol. 64, no. 6, pp. 496–510.

Moeller, M, Pawlowski, S, Petersen-Thiery, M, Miller, IB, Nietzer, S, Heisel-Sure, Y & Schupp, PJ 2021, 'Challenges in current coral reef protection–possible impacts of UV filters used in sunscreens, a critical review', Frontiers in Marine Science, vol. 8, p. 665548.

Rasterelli, G, Rigano, L & Gazzaziga, G 2012, Sunscreen composition comprising hydroxyapatite as physical solar filter.

Reinosa, JJ, Leret, P, Álvarez-Docio, CM, del Campo, A & Fernández, JF 2016, 'Enhancement of UV absorption behavior in ZnO–TiO2 composites', Boletín de la Sociedad Española de Cerámica y Vidrio, vol. 55, no. 2, pp. 55–62.

Roth, WJ, Gil, B, Makowski, W, Marszalek, B & Eliášová, P 2016, 'Layer like porous materials with hierarchical structure', Chemical Society Reviews, vol. 45, no. 12, pp. 3400–3438.

Rozaini, MZH, Hamzah, H, Mohtar, NF, Sainoruddin, MH, Sofian, FRM, Ghazali, MSM & Fei, LC 2017, 'Biomaterials derived from tamban, Sardinella fimbriata bones as promising anodyne sunscreen', Journal of Sustainability Science and Management, vol. 3, pp. 75–84.

Saraf, S & Kaur, CD 2010, 'Phytoconstituents as photoprotective novel cosmetic formulations', Pharmacognosy Reviews, vol. 4, no. 7, p. 1.

Serpone, N 2021, 'Sunscreens and their usefulness: have we made any progress in the last two decades?', Photochemical & Photobiological Sciences, vol. 20, no. 2, pp. 189–244.

Singh, G, Singh, RP & Jolly, SS 2020, 'Customized hydroxyapatites for bone-tissue engineering and drug delivery applications: A review', Journal of Sol-Gel Science and Technology, vol. 94, no. 3, pp. 505–530.

Villalobos-Hernandez, JR & Müller-Goymann, CC 2006, 'Sun protection enhancement of titanium dioxide crystals by the use of carnauba wax nanoparticles: The synergistic interaction between organic and inorganic sunscreens at nanoscale', International Journal of Pharmaceutics, vol. 322, no. 1–2, pp. 161–170.

Wang, Z, Shang, J & Zhang, Z 2025, 'Composite or modified hydroxyapatite microspheres as drug delivery carrier for bone and tooth tissue engineering', Current Medicinal Chemistry, vol. 32, no. 5, pp. 974–981.

Watkins, YS & Sallach, JB 2021, 'Investigating the exposure and impact of chemical UV filters on coral reef ecosystems: Review and research gap prioritization', Integrated Environmental Assessment and Management, vol. 17, no. 5, pp. 967–981.

de Araujo, TS, Macedo, ZS, de Oliveira, PA & Valerio, ME 2007, 'Production and characterization of pure and Cr3+-doped hydroxyapatite for biomedical applications as fluorescent probes', Journal of Materials Science, vol. 42, no. 7, pp. 2236–2243.